Passivation of reinforcing steel in reactive MgO cement blended with Portland cement

Mi, Tangwei; Yang, En-Hua; Unluer, Cise

Published in:
Cement and Concrete Composites

DOI:
10.1016/j.cemconcomp.2023.105269

Publication date:
2023

Cement and Concrete Composites 143 (2023) 105269

Contents lists available at ScienceDirect

Cement and Concrete Composites

journal homepage: www.elsevier.com/locate/cemconcomp

Passivation of reinforcing steel in reactive MgO cement blended with Portland cement

Tangwei Mi [a], En-Hua Yang [a], Cise Unluer [b,*]

[a] School of Civil and Environmental Engineering, Nanyang Technological University, 50 Nanyang Avenue, 639798, Singapore
[b] Department of Mechanical, Aerospace and Civil Engineering, University of Manchester, Manchester, M13 9PL, United Kingdom

ARTICLE INFO

Keywords:
Surface layer
Pore solution
Electrochemical properties
MgO
Blended cement

ABSTRACT

Reactive MgO cement (RMC) has an ability to gain strength by carbonation. One of the main concerns in RMC systems is the potential corrosion of reinforcing steel in structural applications. This study evaluated the feasibility of replacing small proportions of RMC with Portland cement (PC) to promote the passivation of reinforcing steel. Reinforcing steels embedded in RMC with different proportions of PC were investigated by electrochemical measurements and microstructural analysis. Pore solutions extracted from these pastes were evaluated for their chemical compositions. Inclusion of ≥2% PC enabled the passivation of steel. Passive film forming in RMC-PC blends consisted of Fe_3O_4 and $Mg(OH)_2$, which was thicker than those in pure PC mixes. The formation of passive film was mainly attributed to the increased pH of the pore solution, which reached over 12 in RMC mixes containing only 2% PC. These findings highlighted the potential of using RMC mixes in reinforced concrete applications.

1. Introduction

Global cement production accounts for approximately 1.63 billion tons of CO_2, equivalent to around 8% of total anthropogenic emissions, resulting in serious environmental impacts [1]. To mitigate these effects, alternative cementitious materials, one of which is reactive MgO cement (RMC), are being investigated [2–4]. RMC presents certain benefits when compared to ordinary Portland cement (PC), including the relatively low calcination temperature used during its production (700–1000 vs. 1450 °C) via the dry route [4–6] and its capability to be produced from waste resources such as desalination brine via the wet route [7–9]. Additionally, RMC can react with CO_2 and develop strength subsequently [10,11]. The sequestration of CO_2 involves the reaction of brucite with CO_2, resulting in the formation of hydrated magnesium carbonates (HMCs) such as nesquehonite ($MgCO_3{\cdot}3H_2O$), hydromagnesite ($4MgCO_3{\cdot}Mg(OH)_2{\cdot}4H_2O$), dypingite ($4MgCO_3{\cdot}Mg(OH)_2{\cdot}4H_2O$) and artinite ($MgCO_3{\cdot}Mg(OH)_2{\cdot}3H_2O$) [10]. The formation of HMCs reduces the pore space in RMC samples and forms a continuous network, which consequently contributes to strength development. With the involvement of CO_2 sequestration and production optimisation, RMC produced via both dry and wet routes demonstrated a potential to produce less CO_2 emissions than that of PC [7,12,13].

Previous studies looked into enhancing the hydration and carbonation mechanisms of RMC mixes under different curing conditions [11,14–19]. Various strategies were reported to facilitate the carbonation of RMC, including the use of HMCs as cement replacement [11], improvement of the curing conditions [3], and addition of hydration and dispersion agents [20]. Whist the investigation of the mechanical and microstructural properties of RMC has demonstrated its potential as an alternative binder mainly in non-structural applications [16,17,21], the long-term durability of RMC-based mixes has not been studied in detail. In particular, one of the main limitations of carbonated RMC systems is the relatively low pH of the system, raising concerns about the resistance of reinforcing steel embedded in RMC against corrosion in structural applications [22]. The single study that looked into the corrosion resistance of RMC composites reported the corrosion of the reinforcing steel in RMC mixes with and without carbonation [22]. To compare, in PC mixes, a thin passive film forming on the surface of reinforcing steel protects it from the penetration of oxygen and water, thereby preventing corrosion [23]. To form a reliable passive film, a highly alkaline environment (pH of ~12) is essential [24]. Hydration of PC usually generates a pH value of ~13 [25], which is ideal for the formation of passive film. However, passivation of reinforcing steel in RMC is questionable due to the low pH of this system (~9.9–10.5) [16].

* Corresponding author.
E-mail address: cise.unluer@manchester.ac.uk (C. Unluer).

https://doi.org/10.1016/j.cemconcomp.2023.105269
Received 19 January 2023; Received in revised form 22 June 2023; Accepted 22 August 2023
Available online 23 August 2023

Considering that the low pH value of the RMC system restricts the formation of a passive film around the reinforcement, the durability of this system could be improved by increasing its alkalinity. This could be achieved via the addition of a small amount of PC in RMC, which could increase the pH value of the pore solution due to the hydration of alkali/alkali-earth metal oxides (CaO, K_2O and Na_2O) [26]. Furthermore, past research involving the combination of RMC with a small amount of PC demonstrated that these mixes achieved a comparable strength to PC [27–29] and a higher resistance to chemical attack due to their lower porosity [28,30]. Although RMC-PC blends revealed promising results in terms of mechanical performance and microstructural development, their ability to enable the passivation of mild steel has not been explored until now.

In line with this gap in the literature, this study aims to investigate the feasibility of promoting the passivation of embedded reinforcing steel in RMC mixes via the addition of small amounts of PC. To determine effect of different amounts of PC addition on the behaviour of reinforcing steel, mixes where RMC was replaced by 0%, 2%, 20% and 100% PC by mass were investigated. The electrochemical behaviour of reinforcing steel in different mixes was analysed. Subsequently, the pore solutions were extracted from these mixes, and the pH and ion concentrations of the pore solutions were evaluated for comparison. Finally, the microstructure and chemical composition of the corrosion products/passive films were characterized by scanning electron microscopy and Raman spectroscopy. The passivation of the reinforcing steel and the protectivity of the passive film in RMC mixes involving small portions of PC were reported, demonstrating the potential of RMC mixes for structural applications.

2. Methodology

2.1. Materials

RMC used in this work was produced by Lingshou Minerals Processing Plant, sourced from Liaoning, China. The chemical composition of RMC is listed in Table 1. PC was from Lafarge cement Pte. Ltd. (Singapore). The mix compositions are given in Table 2. Four different binder compositions, where the proportions of PC were 0%, 2%, 20% and 100%, were prepared and labelled as M100, M98, M80 and M0, respectively. These levels were determined based on the preliminary tests performed on the pore solution extracted from RMC blended with 2%, 5%, 10%, 20%, 40%, 60%, 80% and 100% PC. These results revealed that the addition of 2% of PC increased the pH value dramatically from ~11.3 to ~12.1; whilst 20% of PC raised the pH value to around 12.5.

2.2. Experimental programme and sample preparation

The overall experimental programme was divided into three steps to investigate the 1) electrochemical behaviour of reinforcing steel, 2) pore solution of different cement paste mixes and 3) corrosion products/passive film formed on reinforcing steel. Accordingly, three types (A, B and C) of paste samples were prepared, as shown in Fig. 1. Fig. 1 (a) shows Type A sample, a self-designed cell for electrochemical measurements, where the reinforcing steel was cut into a disc with a height of ~10 mm that was connected with a copper wire. Both the reinforcing steel and copper wires were sealed by epoxy with only cross section of reinforcing steel exposed to the paste. This enabled the control of not only the exposure area but also the setup of the three electrodes system. More importantly, the reinforcing steel sample could be taken out from the cell after 28 days for microscale analysis. A picture of the assembled cell can be seen in Fig. 1 (b). Fig. 1 (c) shows the model for the Type B paste sample used for pore solution extraction, which was designated for the one-dimension mechanical squeezing device. After immersion in the paste for 28 days, the assembled sample shown in Fig. 1 (b) was taken out from the cell as shown in Fig. 1 (d), and used in scanning electron microscopy (SEM) and Raman spectroscopy analyses to study the microstructure and chemical composition of corrosion products/passive films. Fig. 1 (e1) shows the Type C paste sample prepared for the investigation of the cross-section of the passive film by SEM with energy dispersive X-ray (EDX). The detailed processes are shown in Fig. 1 (e2-3), where the lateral surface of reinforcing steel (pointed by the blue arrow in Fig. 1 (e2)) was initially polished and fully embedded in the paste for 28 days before analysis. On the day of analysis, the surface of the whole assembled sample was polished so that the interface of the paste and reinforcing steel can be exposed for analysis, as depicted in Fig. 1 (e3).

Table 1
Chemical composition of RMC.

Chemical compositions	MgO	CaO	SiO_2	Al_2O_3	Fe_2O_3	SO_3
Weight (%)	94.4	1.6	2.8	0.5	0.5	0.2

Table 2
Mix compositions of mixes prepared in this study.

Mix	Binder composition		Water to binder (w/b) ratio
	RMC (%)	PC (%)	
M100	100	0	0.5
M98	98	2	
M80	80	20	
M0	0	100	

2.3. Electrochemical measurements

A potentiostat from Princeton Applied Research (USA) was employed to perform electrochemical measurements. The electrochemical setup consisted of three electrodes, with reinforcing steel as the working electrode, a platinum counter electrode and a saturated calomel reference electrode, as shown in Fig. 1 (a). Open circuit potential (OCP) was recorded every 5 s for 5 min at 0d, 1d, 3d, 7d, 14d and 28d. Electrochemical impedance spectrum (EIS) measurements were performed within the frequency range of 100 kHz to 0.01 Hz at 7d and 28d, with an AC signal of amplitude 10 mV.

2.4. Measurements related to pore solution

After Type B paste samples were cured for 24 h, they were inserted into a one-dimension mechanical squeezing device under a pressure of <100 MPa to extract the pore solution from different mixes. The pore solution from each mix was separated into two tubes for ICP-OCE and pH measurements and sealed until analysis. ICP-OES (PerkinElmer Optima DV2000) was employed to measure the ion concentration of the pore solution. The pH value of the solution was measured by a METTLER pH probe. In addition to the pH value at 24h, the pH evolutions of the fresh pastes within the first 4 h were also monitored.

2.5. Measurements related to corrosion product and passive film

2.5.1. Microstructural analysis

A Zeiss Evo 50 microscopy was used to study the microstructure of corrosion products and passive films. The elemental distributions were characterized by EDX with an accelerating voltage of 15 kV and a working distance of 15 mm. All samples were dried in vacuum and mounted onto sample stage by using double-sided adhesive carbon tape.

2.5.2. Raman spectroscopy

The corrosion products and passive films were characterized by Raman spectroscopy after the reinforcing steels were embedded in pastes for 28 days. To avoid possible transformation of the corrosion products/passive films, the reinforcing steel was taken out just before

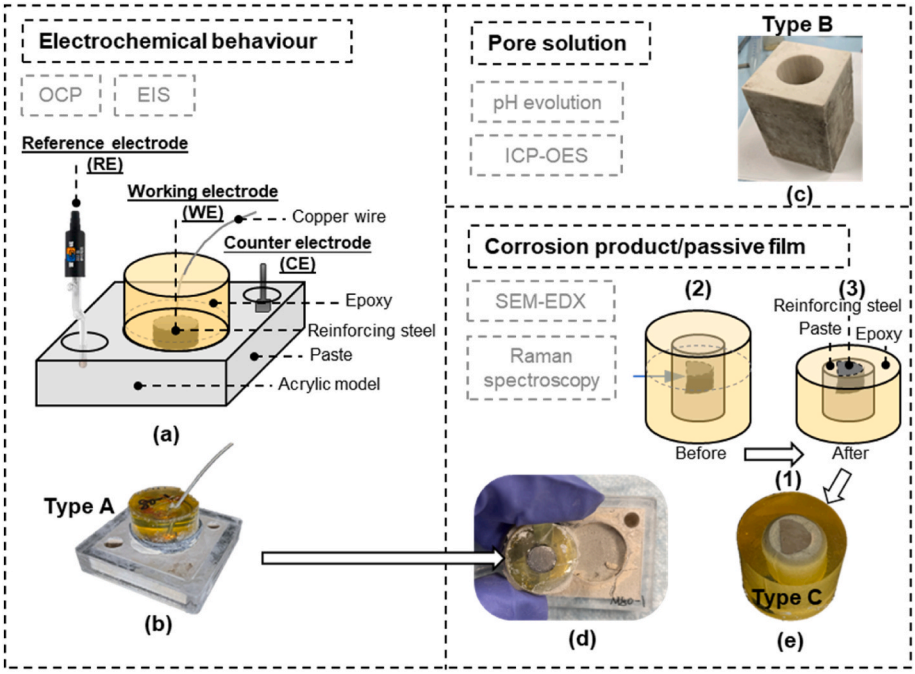

Fig. 1. Experimental programme showing sample preparation and measurement setup.

the Raman tests, and the laser power was limited within 5% of the maximum power. A Renishaw Raman spectroscope equipped with a 785 nm laser was employed. The laser was focused via a Lecia 50 × (N.A. = 0.55) into a spot size of ~1.5 μm. All the spectra were recorded with an exposure time of 30s and 2 accumulations. The final results were obtained by taking the average results of three spectra collected from the corrosion products/passive films. To facilitate the comparison between different spectra, their backgrounds were eliminated by using baseline correction (OriginPro).

3. Results

3.1. Electrochemical results

OCP is the equilibrium potential between the reinforcing steel and reference electrode without applied load, indicating the passivation/corrosion state of the reinforcing steel [31]. The OCP values of the reinforcing steels in different mixes are shown in Fig. 2. For the reinforcing steel in M100 paste, the OCP value started at around −450 mV, which decreased to −500 mV on the 3rd day and increased gradually afterward to ~ -400 mV on the 28th day. Overall, the OCP values were within a relatively low range, revealing the corrosion state of the reinforcing steel in M100 paste [32–34]. The OCP values of the reinforcing steels in M98, M80 and M0 all increased gradually to above −200 mV on the 28th day, suggesting the formation of a passive film on these steels. Remarkably, the steel in M98 achieved the highest OCP values after 3 days, implying that the passive film formed in M98 probably had a higher resistance. These results could potentially indicate the variations in the passive films forming in M98, M80 and M0 pastes, such as their chemical composition and thickness [32].

EIS spectra, shown in Fig. 3, were collected on day 7 and 28, in order

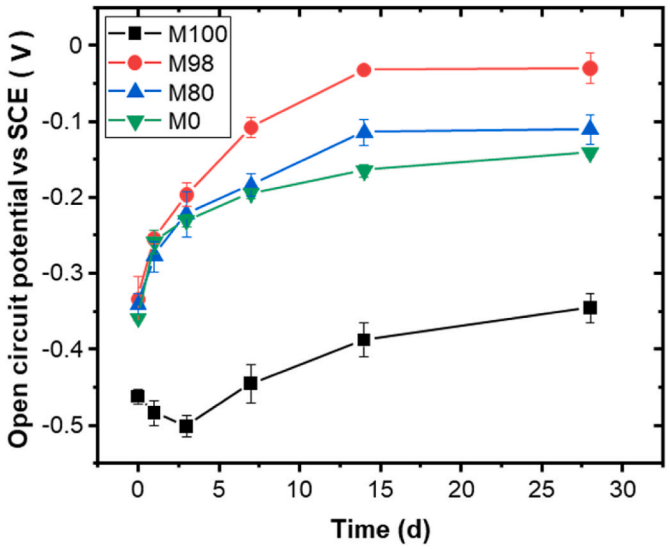

Fig. 2. OCP results of reinforcing steel exposed to different mixes.

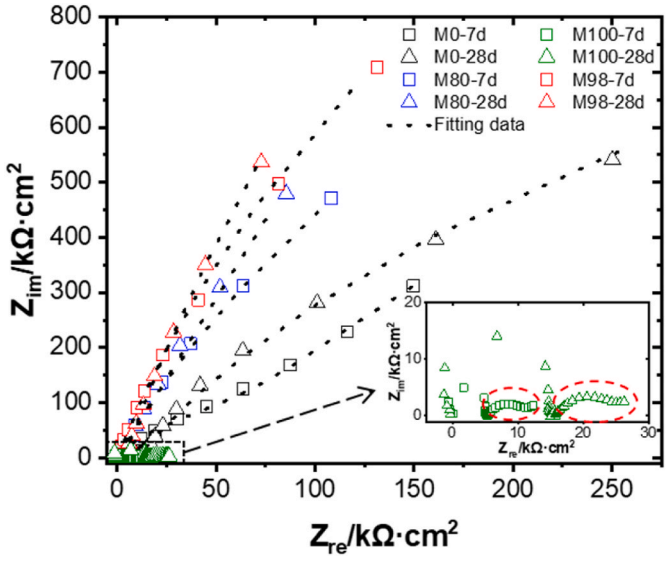

Fig. 3. EIS results of reinforcing steel exposed to different mixes and corresponding fitting data.

to further investigate the passivation or corrosion behaviours of the reinforcing steels. The semi-circle diameters of the Nyquist plots, representing the polarization resistance of the mild steel, was found to be highest in M98 paste and lowest in M100 paste (as indicated in red circles in Fig. 3). The extremely low value of the semi-circle diameter for the sample in M100 paste indicated its corrosion state, which was in agreement with the OCP results. To further evaluate the passivation behaviour of the samples in M98, M80 and M0, an equivalent element circuit (EEC) (shown in Fig. 4) was chosen, depicting the EIS data. In the EEC model, R_c represents the resistance of the cement paste cover; R_f and Q_f are the resistance and capacitance of the passive film, respectively; and R_{ct} and Q_{dl} are attributed to the charge transfer resistance and capacitance of the double layer at steel/paste interface. Constant phase elements (CPE) (for Q_f and Q_{dl}) were employed to replace ideal capacitator due to the irregularities of steal surface and surface roughness [35] and non-uniform thickness of the passive film [36].

The fitting curves are plotted in Fig. 3 and the calculated results are listed in Table 3. In general, there is an apparent increase of resistance from day 7–28 in all mixes, indicating the growth of the passive film [37]. By comparing the resistance among the samples subjected to different pastes, it can be found that R_c value of sample in M0 (i.e. pure PC paste) was the highest among all pastes. However, in the same paste (M0), the resistance of passive film (R_f) exhibited the lowest value on both day 7 and 28, which can be corresponding to its lowest OCP values. In terms of the charge transfer resistance, all samples revealed comparable values, indicating that the passive films formed in M98, M80 and M0 showed similar resistance to corrosion.

In conclusion, the corrosion of reinforcing steel was found in M100 paste, which was in agreement with the findings of previous studies [22]. In the paste containing 2% PC (M98), the passivation of reinforcing steel was noted. When compared with the reinforcing steels in the other pastes (M80 and M0), the OCP value in M98 was the highest. In the EIS fitting results, the resistance of the passive film in M98 was the highest, whilst the charge transfer resistances of all passivated samples were comparable to each other.

3.2. Analysis of the pore solution

The ion concentrations of the pore solutions after 1 day were analysed and the results are shown in Table 4. The highest Mg ion concentration (6.35 mg/L) was detected from the pore solution of M100, which also contained 18.25 mg/L Ca ions sourced from the small amount of CaO present in RMC, as shown in Table 1. The concentration of Ca ions was higher than that of Mg ions, which could be attributed to the higher solubility of $Ca(OH)_2$ than that of $Mg(OH)_2$ [38,39]. In the pore solutions of M98 and M80, Mg ions were dramatically reduced, and the other ions, Ca, Na and K, were increased due to the addition of PC. The reduction of Mg ions was attributed to increase in the pH value, i.e. the increase of OH^- concentration. As the solubility product constant, K_{sp} (in Equation (1), is invariable at different temperatures [40], the increase of OH^- ions would thus reduce the concentration of Mg ions in the solution. These Mg ions could precipitate as $Mg(OH)_2$ on the surface of reinforcing steel [41]. In the pore solution of M0, the concentrations of Na and K ions were both higher than those in other samples. The concentration of Ca ions in the pore solution of M0 (i.e. sample with the highest CaO content) was lower than those in M98 and M80. As shown in Equation (2), an increase in the pH value led to a rise in OH^- concentration and thus reduced Ca ions. These significant differences among the pore solution of each sample could explain the variations in their electrochemical behaviours [42].

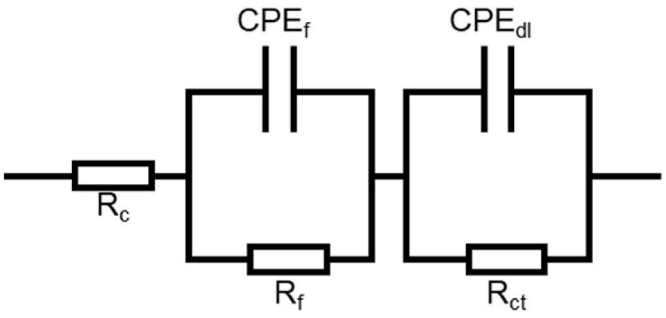

Fig. 4. Electrochemical equivalent circuit to fit EIS results.

Fig. 5 presents the pH value evolution of the pore solution in pastes M0, M80, M98 and M100. All pH values increased sharply during the first 3 h, followed by gradual increases, which was in line with the previous observations [43,44]. After 24 h, the pH value of M100, i.e. pure RMC, was ~11.3. With addition of 2% PC (M98), the pH value of the pore solution was increased to 12.1 after 24 h. With a further increase in PC proportion, the pH values of the pore solutions increased to 12.5 and 13.1 after 24 h for M80 and M0, respectively [45–47].

The formation of a passive film normally takes place in alkaline environments [24]. However, the pH value threshold reported in previous work for the formation passive film varied [32,34,48]. For instance, corrosion of iron was noted in a solution with a pH of ~11.5 [32], whilst passive film formed in a solution with a pH value of ~12.0 [24]. In present work, it can be seen that the initial pH value of M100 was ~10.3, which was much lower than the threshold for the passivation of reinforcing steel, thereby resulting in the formation of corrosion products in early stages. Though the pH value increased gradually to 11.3, this was still not sufficient to form a steady passive film [24]. For the remaining pore solutions in M98, M80 and M0, the pH values all reached >12, passivating the embedded reinforcing steels.

$$Mg(OH)_{2\ (s)} \leftrightharpoons Mg^{2+}_{(aq)} + 2OH^-_{(aq)}\ K_{sp} = [Mg^{2+}][OH^-]^2 \quad (1)$$

$$Ca(OH)_{2\ (s)} \leftrightharpoons Ca^{2+}_{(aq)} + 2OH^-_{(aq)}\ K_{sp} = [Ca^{2+}][OH^-]^2 \quad (2)$$

3.3. Corrosion products and passive film

3.3.1. SEM-EDX

After steel was embedded into different types of pastes, the surfaces of samples were taken out each paste were studied under SEM, as shown in Fig. 6. The steel embedded in M100 was corroded with dark yellow corrosion products, whilst no corrosion products could be found on the other surfaces. When compared with the glossy steel surface embedded in M0, samples in M98 and M80 were matting with several paste particles.

SEM images shown in Figs. 7 and 8 provide a comparison for the microstructures of corrosion products and passive film. Various morphologies, resembling a worm nest, bird's nest and globular shapes with loose and porous microstructures were observed in Fig. 7, which were attributed to different formations of lepidocrocite, as observed in previous work [49]. Fig. 8 shows the SEM images of samples in Fig. 6 (b)–(d). Along with the white particles that indicated the presence of residual paste scattered around the surfaces of the steel in M98 (Fig. 8 (a)) and M80 (Fig. 8 (b)), these samples were slightly smoother than those in M0 (Fig. 8 (c)). The lower visibility of the scratches in the former ones, especially M98, could refer to the thicker formation of a film on the steel surface, thereby covering the scratches and resulting in a smoother surface.

SEM-EDX was employed to investigate the thickness of passive films in M80 and M98, whose results are shown in Figs. 9 and 10, respectively. The passive film forming in M0 (pure PC) was not detected due to its extremely thin thickness, reported to be ~10 nm [50,51]. Fig. 9 shows the interface between steel and M80 paste, where the passive film could be clearly identified by the distribution of O and Fe, revealing an average thickness of ~4.44 μm. The passive film forming in M98, as shown in Fig. 10, had a thickness of ~12.5 μm. In addition to Fe ions, Mg was also found within the passive films in both M98 and M80.

Table 3
Fitting results showing the value of each electrical element in different samples.

	Rc (kΩ·cm^2)	Qf; Y_0 ($\Omega^{-1}\cdot s^n/cm^2$)	Qf; n	Rf (kΩ·cm^2)	Qdl; Y_0 ($\Omega^{-1}\cdot s^n/cm^2$)	Qdl; n	Rct (kΩ·cm^2)
M0-7d	8.64	2.47E-03	0.85	1.57E+03	5.93E-05	1.00	6.41E+04
M0-28d	12.61	1.71E-03	1.00	6.29E+03	8.87E-05	0.80	7.59E+04
M80-7d	2.52	2.56E-03	0.80	5.14E+04	2.74E-03	0.80	6.35E+04
M80-28d	4.40	1.59E-01	0.91	6.14E+04	2.57E-02	0.80	7.99E+04
M98-7d	3.34	1.95E-02	0.43	6.28E+04	6.35E-02	0.95	6.42E+04
M98-28d	8.91	7.74E-02	0.92	7.76E+04	2.37E-03	0.80	8.05E+04

Table 4
Ion concentrations in the pore solutions extracted from different mixes.

Ion(mg/L) Paste	Mg	Ca	K	Na
M100	6.35	18.25	2.02	1.28
M98	0.64	126.30	111.78	59.80
M80	0.04	111.70	273.80	150.38
M0	0.00	20.98	1257.20	438.60

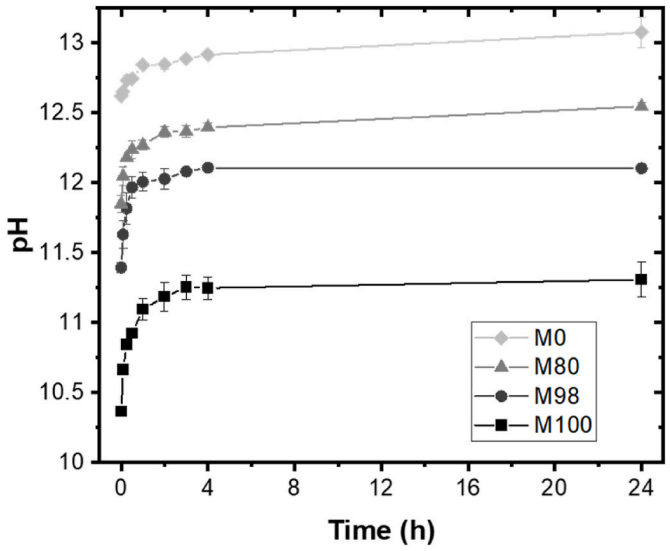

Fig. 5. pH evolutions of the pore solutions extracted from different mixes.

In summary, corrosion products were clearly visible on the steel exposed to M100 paste, resulting in a loose and porous structure; whilst the steels embedded in the other pastes exhibited a passive state without any corrosion products. Significant differences in the thickness of the passive film forming on the steel surface exposed to different pastes were observed, which were noted as ~10 nm in M0 [50,51], ~4.44 μm in M80 and ~12.5 μm in M98.

3.3.2. *Raman results*

Following the SEM and EDX measurements, Raman spectroscopy was employed to identify the chemical compositions of the corrosion products and passive films. Fig. 11 shows an average Raman spectrum obtained from the corrosion products on the surface of the steel in M100 paste. The Raman spectrum presented two sharp peaks at 250 cm^{-1} and 377 cm^{-1}, along with a small peak at 526 cm^{-1}, which are the characteristic peaks of γ-FeOOH [49,52,53]. This was in line with the images shown in Fig. 7, confirming that the corrosion product was γ-FeOOH. The Raman spectra obtained from the passive films in M98, M80 and M0 are shown in Fig. 12. The spectrum labelled M0 at the bottom only exhibited a small peak at ~667 cm^{-1}, which should be attributed to the stretching vibrational mode along Fe–O bond in the tetrahedral sites of Fe_3O_4 [54–58]. Therefore, the main composition of the passive films formed in M0 (pure PC) could be Fe_3O_4, which was consistent with previous observations [59,60]. Alternatively, the Raman spectra observed in the passive films in M98 and M80 presented three additional Raman peaks at around 278, 441 and 520 cm^{-1}, suggesting the presence of $Mg(OH)_2$ that was thoroughly attached to the passive film [61–64]. The intensities of the peaks of the spectrum observed in M98 were higher than those in M80, which could be caused by the thicker passive film forming in M98. Therefore, differences in the chemical composition of the corrosion products and passive film were noted, which were γ-FeOOH and Fe_3O_4, respectively. Specifically, the passive films forming in M98 and M80 contained $Mg(OH)_2$, which differed from the one observed in M0.

4. Discussion

The experimental results presented in this work have revealed the potential of using steel reinforcement in RMC mixes via the introduction of small amounts of PC. Based on the obtained results, the corrosion/passivation of reinforcing steel in the mix formulations investigated in this study is demonstrated in Fig. 13. In M100 (pure RMC) paste, due to the low initial pH value of the pore solution (pH = 10.3), passive film could be hardly form, presenting a suitable environment for corrosion. In a low pH environment, the main composition of the corrosion product is lepidocrocite, which was supported by the results in this study as well as the literature [65]. As depicted in Fig. 13 (a), lepidocrocite is a layered structure [66], which is loose and non-protective [67,68].

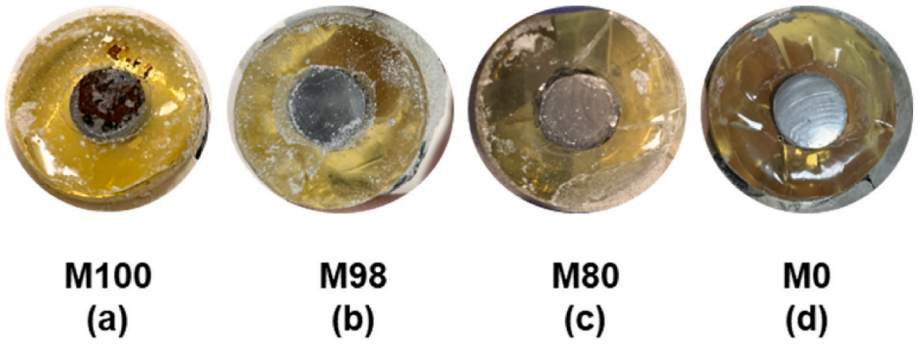

Fig. 6. The surfaces photos of the reinforcing steel after being embedded in (a) M100, (b) M98, (c) M80 and (d) M0 pastes for 28 days.

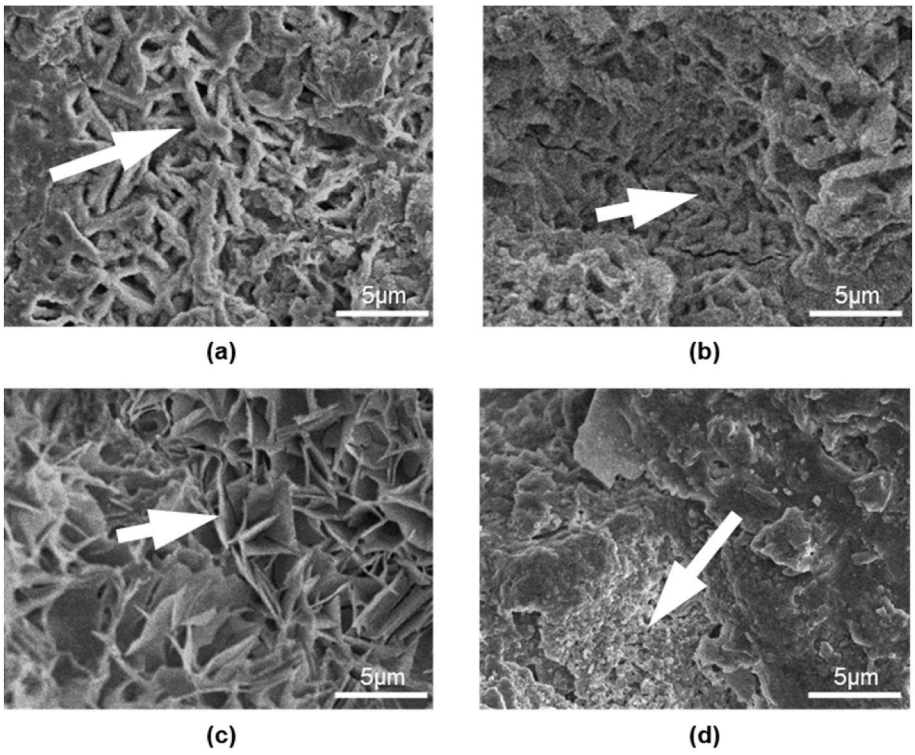

Fig. 7. The morphology of the rust on the surface of the reinforcing steel exposed to M100, showing different formations of lepidocrocite, (a) and (b) worm nest; (c) bird's nest and (d) globular shapes.

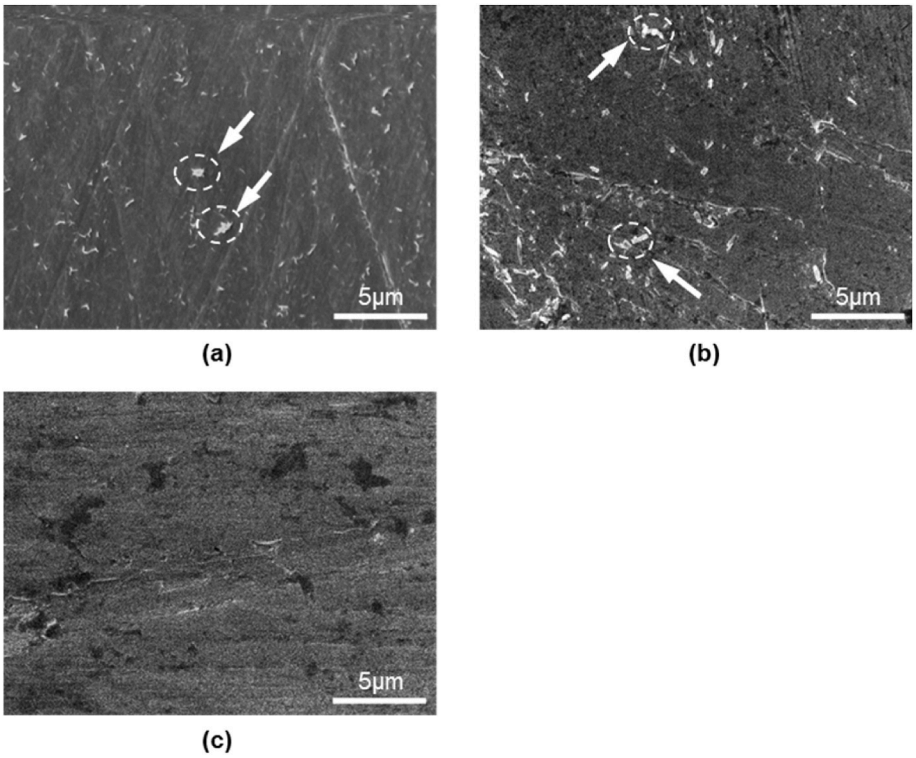

Fig. 8. The morphology of the surface of reinforcing steel exposed to (a) M98, (b) M80 and (c) M0 pastes.

Alternatively, in the other samples (M98, M80 and M0), the higher pH values of the pore solution could enable the formation of a passive film [24,69]. However, the thickness and chemical composition of the passive film differed across samples. The passive film was composed of Fe_3O_4, as supported by the Raman results and previous findings [59,70,71]. As shown in Fig. 13, Fe_3O_4 has an inverse spinel crystal structure with the oxygen atoms forming a face-centred cubic close-packing lattice [72], which could form a thin and dense film to protect the substrate

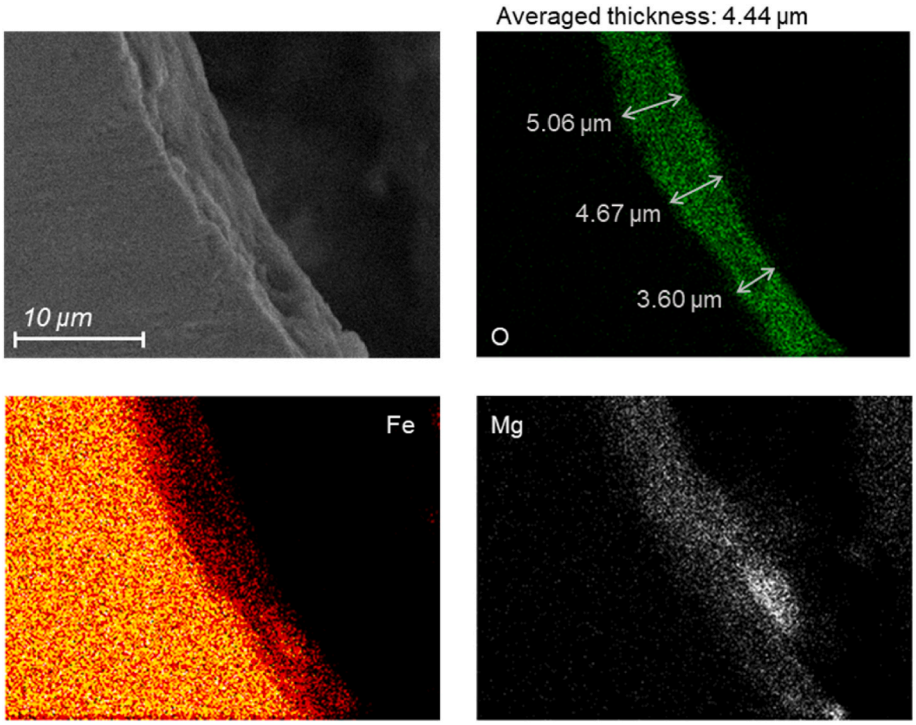

Fig. 9. SEM-EDX results showing the passive film formed on reinforcing steel in M80 paste.

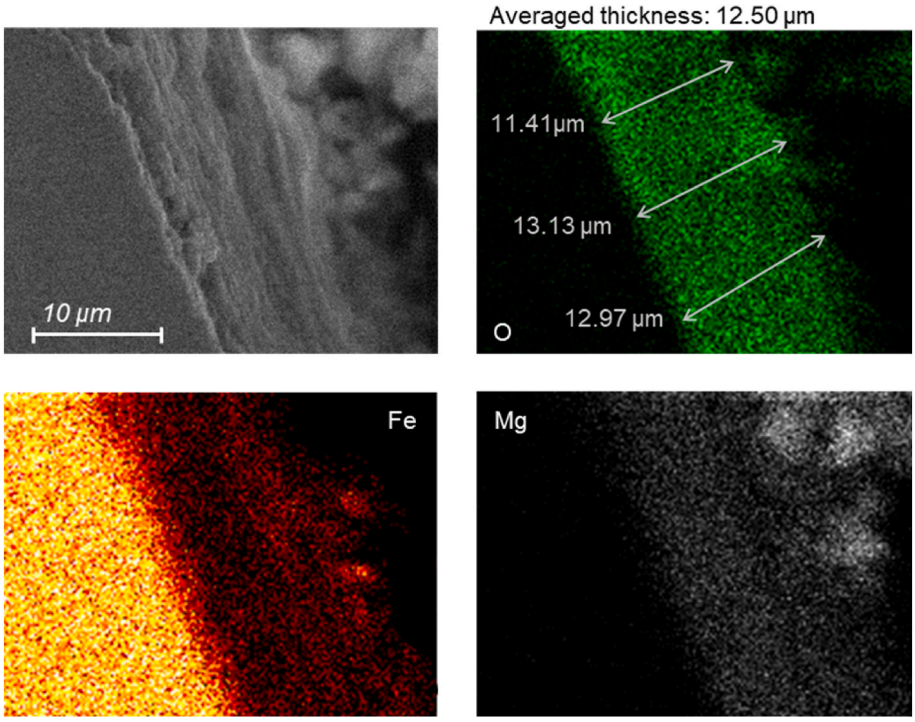

Fig. 10. SEM-EDX results showing the passive film formed on reinforcing steel in M98 paste.

[73]. In addition to Fe_3O_4, $Mg(OH)_2$ was also present in the passive films forming in M98 and M80, introducing a layered and relatively more porous structure [74]. Therefore, the passive films forming in M98 and M80 were not as dense as that observed in M0. In addition to density, another aspect where the passive films differed from each other was their thickness, which was ~12.50 μm and ~4.44 μm in M98 and M80, respectively. These were notably thicker than the film that formed in M0 (~10 nm [50,51]). The higher thickness could be attributed to the co-presence of Fe_3O_4 and $Mg(OH)_2$. The differences in the passive films could be linked with the variation in pH of the surrounding environment [24,69]. Accordingly, the reaction rate of iron to form iron (II, III) ion is highly dependent on pH value, which increases dramatically with the decrease of pH [75]. The fast dissolution of iron in M98 and M80 could have promoted its diffusion from the surface, coupled with the

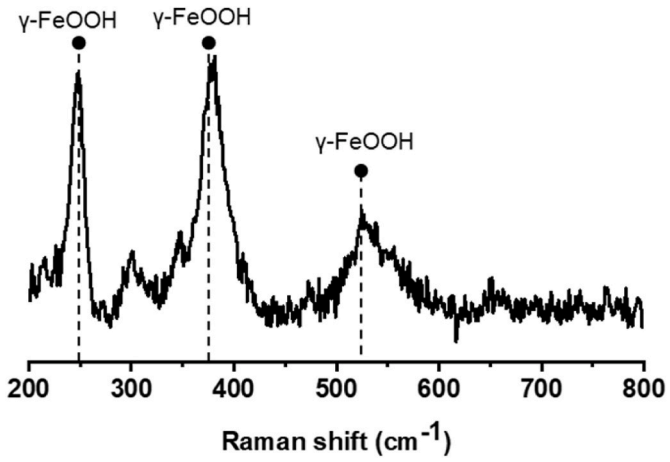

Fig. 11. Raman spectrum obtained from the corroded reinforcing steel in M100 paste.

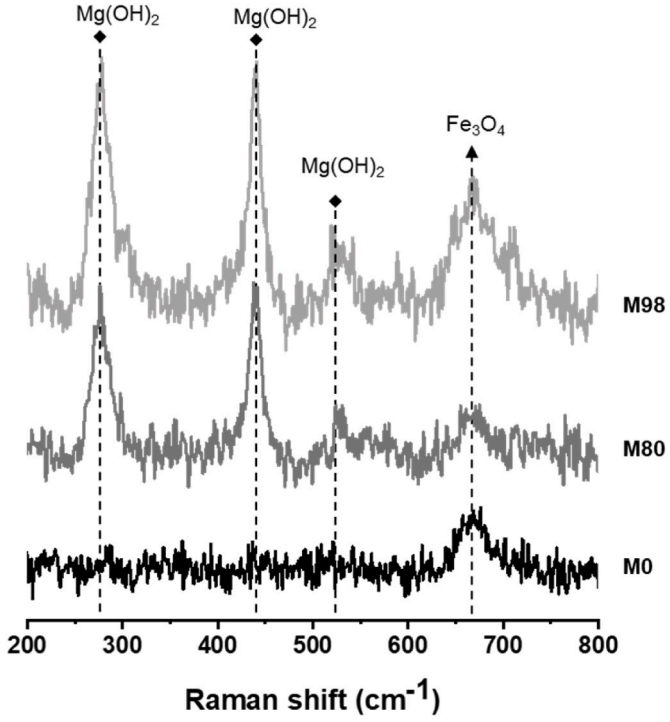

Fig. 12. Raman spectra obtained from the reinforcing steels exposed to M98, M80 and M0 pastes.

co-existence of $Mg(OH)_2$, resulting in a thicker film. Although the passive films forming in M98 and M80 were much thicker than that forming in M0, their resistance to corrosion were comparable due to the less dense structure of the former, associated with the formation of $Mg(OH)_2$ with a porous structure.

Another factor that plays a key role in the corrosion/passivation of the reinforcing steel in RMC pastes is the composition of the binder itself. While the pH of RMC paste was reported as ~10.5 [76], the corresponding value of RMC paste in this study was measured as ~11.3, which was attributed to the presence of CaO (1.6%) in the raw material. The results revealed that the addition of 2% of PC could promote the formation of passive film, which was mainly caused by the increase of the pH value of the pore solution [24,69]. Alternatively, the reinforcing steel could be passivated in pure RMC pastes by merely increasing the content of CaO or other alkali metal oxides, such as K_2O and Na_2O, during the production process or afterward. Considering that RMC can also be obtained from alternative routes (e.g. reject brine) that intrinsically contain various amounts of alkali metal oxides during the extraction process [7], these routes involving by-products could be explored for the production of RMC compatible with steel reinforcement.

The carbonation of the system was not considered in this primary work. The initial carbonation reaction on the surface of RMC can lead to the formation of a dense carbonate layer, which may act as a barrier against the penetration of additional CO_2 towards the steel reinforcement [77]. Consequently, the pH value around the reinforcing steel may not be significantly affected as the CO_2 diffusion in the vicinity of the reinforcement is limited, thereby enabling the steel to remain passivated. Thus, in the initial stages, the passivation behaviour of the steel reinforcement is independent of carbonation. As a result, the present study primarily focused on evaluating the potential for the passivation of the steel reinforcement in RMC-PC blended cement prior to carbonation. However, the corrosion of the reinforcing steel is a possibility due to long-term carbonation [78]. This can be addressed via a further investigation of the properties of the reinforcing steel in M98, M80 pastes under carbonation conditions.

5. Conclusion

This study thoroughly investigated the behaviour of reinforcing steel in RMC pastes blended with different amounts of PC, with an attempt to identify the feasibility of using RMC in structural applications. The main findings are concluded as below.

- Corrosion of the reinforcing steel embedded in pure RMC paste (M100) was observed. Alternatively, steel embedded in M98, M80 and M0 were all passivated, suggesting that addition of 2% PC could enable the formation of passive film.
- The resistance of the passive film varied significantly and was highest in M98 and lowest in M0. However, the charge transfer resistances of all passivated samples were comparable to each other, suggesting a similar resistance to corrosion.
- The corrosion product had porous structure, which mainly consisted of γ-FeOOH. Alternately, smooth surfaces were observed on the reinforcing steels in M98, M80 and M0.
- The thickness of passive films forming in M98 and M80 were around 4.44 and 12.50 μm, respectively. These were much thicker than the film in M0. The composition of the passive film forming in M0 was Fe_3O_4, whereas $Mg(OH)_2$ was found alongside Fe_3O_4, within the passive films in M98 and M80.

The results obtained in this study revealed the potential of RMC to be used in structural applications via the introduction of small amounts of PC to ensure the formation of passive film on reinforcing steel. Further investigation on the behaviour of reinforcing steel in RMC containing minor amounts of PC under carbonation is needed before these blended cements can be used in structural applications.

Credit author statement

T. Mi: Conceptualization, Methodology, Formal analysis, Writing - Original Draft. **E.H. Yang:** Conceptualization, Methodology, Writing - Review & Editing, Supervision. **C. Unluer:** Conceptualization, Methodology, Writing - Review & Editing, Supervision.

Declaration of competing interest

None.

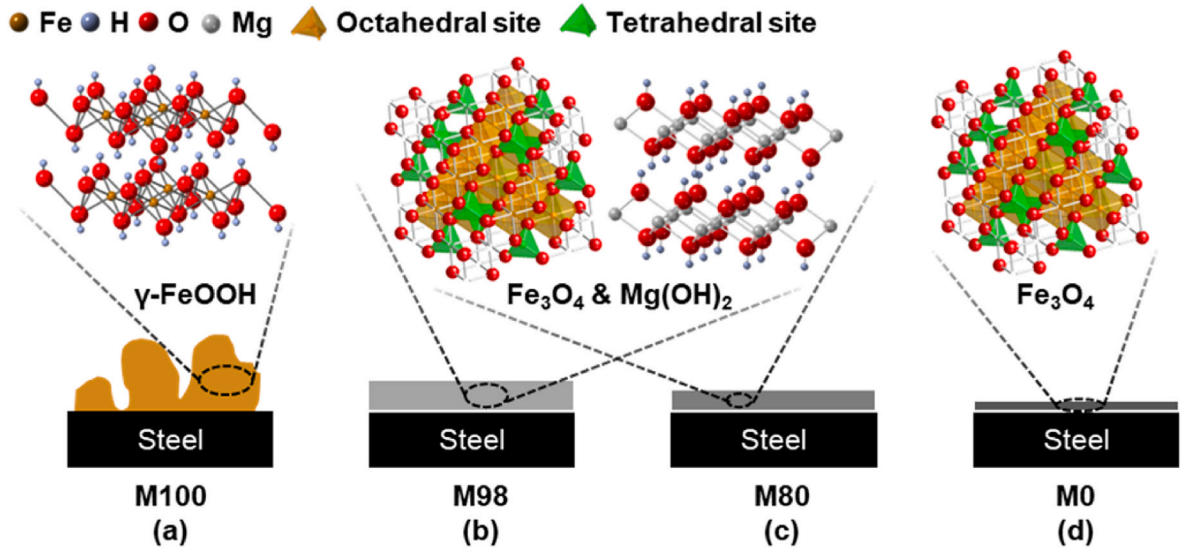

Fig. 13. A schematic showing the corrosion/passivation of reinforcing steel embedded in different mixes.

Data availability

No data was used for the research described in the article.

Acknowledgements

The authors would like to acknowledge financial support from the Ministry of National Development, Singapore (CoT-V1-2020-1).

References

[1] H. Ritchie, M. Roser, P. Rosado, CO_2 and Greenhouse Gas Emissions, 2020.
[2] L. Vandeperre, M. Liska, A. Al-Tabbaa, Hydration and mechanical properties of magnesia, pulverized fuel ash, and portland cement blends, J. Mater. Civ. Eng. 20 (5) (2008) 375–383.
[3] C. Unluer, A. Al-Tabbaa, Enhancing the carbonation of MgO cement porous blocks through improved curing conditions, Cement Concr. Res. 59 (2014) 55–65.
[4] F. Jin, A. Al-Tabbaa, Characterisation of different commercial reactive magnesia, Adv. Cement Res. 26 (2) (2014) 101–113.
[5] S.A. Walling, J.L.J.C.r. Provis, Magnesia Based Cem.: a journey of 150 years, and cements for the future? 116 (7) (2016) 4170–4204.
[6] L. Huang, G. Cheng, S.J.M. Huang, Effects of calcination conditions on the formation and hydration performance of high-alite white portland cement, Clinker 13 (3) (2020) 494.
[7] S. Ruan, E.-H. Yang, C. Unluer, Production of reactive magnesia from desalination reject brine and its use as a binder, J. CO2 Util. 44 (2021), 101383.
[8] H. Dong, C. Unluer, E.-H. Yang, A. Al-Tabbaa, Synthesis of reactive MgO from reject brine via the addition of NH4OH, Hydrometallurgy 169 (2017) 165–172.
[9] H. Dong, C. Unluer, E.-H. Yang, A. Al-Tabbaa, Recovery of reactive MgO from reject brine via the addition of NaOH, Desalination 429 (2018) 88–95.
[10] N.T. Dung, C. Unluer, Sequestration of CO2 in reactive MgO cement-based mixes with enhanced hydration mechanisms, Construct. Build. Mater. 143 (2017) 71–82.
[11] C. Unluer, A. Al-Tabbaa, Impact of hydrated magnesium carbonate additives on the carbonation of reactive MgO cements, Cement Concr. Res. 54 (2013) 87–97.
[12] S. Ruan, C. Unluer, Comparative life cycle assessment of reactive MgO and Portland cement production, J. Clean. Prod. 137 (2016) 258–273.
[13] F. Shahbaz, I. Singh, P. Krishnan, K. Celik, Life cycle assessment of brucite and synthetic MgO produced from reject brine using different alkalis, J. Clean. Prod. 380 (2022), 135071.
[14] N.T. Dung, C. Unluer, Advances in the hydration of reactive MgO cement blends incorporating different magnesium carbonates, Construct. Build. Mater. 294 (2021), 123573.
[15] T. Hoang, N.T. Dung, C. Unluer, J. Chu, Use of microbial carbonation process to enable self-carbonation of reactive MgO cement mixes, Cement Concr. Res. 143 (2021), 106391.
[16] N.T. Dung, C. Unluer, Performance of reactive MgO concrete under increased CO2 dissolution, Cement Concr. Res. 118 (2019) 92–101.
[17] N.T. Dung, C. Unluer, Development of MgO concrete with enhanced hydration and carbonation mechanisms, Cement Concr. Res. 103 (2018) 160–169.
[18] C. Sonat, C. Unluer, Investigation of the performance and thermal decomposition of MgO and MgO-SiO2 formulations, Thermochim. Acta 655 (2017) 251–261.
[19] L. Pu, C. Unluer, Investigation of carbonation depth and its influence on the performance and microstructure of MgO cement and PC mixes, Construct. Build. Mater. 120 (2016) 349–363.
[20] N.T. Dung, C. Unluer, Improving the performance of reactive MgO cement-based concrete mixes, Construct. Build. Mater. 126 (2016) 747–758.
[21] N.T. Dung, A. Lesimple, R. Hay, K. Celik, C. Unluer, Formation of carbonate phases and their effect on the performance of reactive MgO cement formulations, Cement Concr. Res. 125 (2019), 105894.
[22] R. Hay, K. Celik, Hydration, carbonation, strength development and corrosion resistance of reactive MgO cement-based composites, Cement Concr. Res. 128 (2020), 105941.
[23] H.T. Cao, L. Bucea, V. Sirivivatnanon, Corrosion rates of steel embedded in cement pastes, Cement Concr. Res. 23 (6) (1993) 1273–1282.
[24] D.Z. Tang, Y.X. Du, M.X. Lu, Y. Liang, Z.T. Jiang, L.J.M. Dong, Corrosion, Effect of pH value on corrosion of carbon steel under an applied alternating current, Mater. Corrosion 66 (12) (2015) 1467–1479.
[25] R.R. Lloyd, J.L. Provis, J.S.J.C. Van Deventer, C. Research, Pore solution composition and alkali diffusion in inorganic polymer cement 40 (9) (2010) 1386–1392.
[26] H. Chen, P. Feng, S. Ye, W. Sun, The coupling effect of calcium concentration and pH on early hydration of cement, Construct. Build. Mater. 185 (2018) 391–401.
[27] L. Mo, F. Zhang, M. Deng, Effects of carbonation treatment on the properties of hydrated fly ash-MgO-Portland cement blends, Construct. Build. Mater. 96 (2015) 147–154.
[28] L. Wang, L. Chen, J.L. Provis, D.C.W. Tsang, C.S. Poon, Accelerated carbonation of reactive MgO and Portland cement blends under flowing CO2 gas, Cem. Concr. Compos. 106 (2020), 103489.
[29] F. Zhang, Magnesium Oxide Based Binders as Low-Carbon Cements, Imperial College London, 2013.
[30] L. Mo, M. Liu, A. Al-Tabbaa, M. Deng, Deformation and mechanical properties of the expansive cements produced by inter-grinding cement clinker and MgOs with various reactivities, Construct. Build. Mater. 80 (2015) 1–8.
[31] A. Siddaiah, A. Kasar, R. Ramachandran, P.L. Menezes, Chapter 1 - introduction to tribocorrosion, in: A. Siddaiah, R. Ramachandran, P.L. Menezes (Eds.), Tribocorrosion, Academic Press, 2021, pp. 1–16.
[32] X.-H. Sun, X.-B. Zuo, G.-J. Yin, K. Jiang, Y.-J. Tang, Electrochemical and microscopic investigation on passive behavior of ductile iron in simulated cement-mortar pore solution, Construct. Build. Mater. 150 (Supplement C) (2017) 703–713.
[33] X. Yu, S. Al-Saadi, X.-L. Zhao, R.S.J.M. Raman, Electrochemical investigations of steels in seawater sea, Sand Concr. Environ. 14 (19) (2021) 5713.
[34] B. Huet, V. L'Hostis, F. Miserque, H. Idrissi, Electrochemical behavior of mild steel in concrete: influence of pH and carbonate content of concrete pore solution, Electrochim. Acta 51 (1) (2005) 172–180.
[35] M. Criado, D.M. Bastidas, S. Fajardo, A. Fernández-Jiménez, J.M. Bastidas, Corrosion behaviour of a new low-nickel stainless steel embedded in activated fly ash mortars, Cem. Concr. Compos. 33 (6) (2011) 644–652.
[36] L. Liu, S. Li, Z. Gao, H. Jia, Y. Wu, W.J.I. Hu, Effects of chloride and pH on passivation characteristics of Q235 steel in, Simulat.Concr. Pore Solut. 17 (220648) (2022) 2.
[37] V.A. Alves, C.M.A. Brett, Characterisation of passive films formed on mild steels in bicarbonate solution by EIS, Electrochim. Acta 47 (13) (2002) 2081–2091.
[38] R.C. Ropp, Chapter 3 - group 16 (O, S, Se, Te) alkaline earth compounds, in: R. C. Ropp (Ed.), Encyclopedia of the Alkaline Earth Compounds, Elsevier, Amsterdam, 2013, pp. 105–197.

[39] K. Safavi, T.A. Nakayama, Influence of mixing vehicle on dissociation of calcium hydroxide in solution, J. Endod. 26 (11) (2000) 649–651.
[40] J.S.J. Schmuckler, Solubility product constant, Ksp 59 (3) (1982) 245.
[41] N. Um, T. Hirato, Precipitation behavior of Ca(OH)2, Mg(OH)2, and Mn(OH)2 from CaCl2, MgCl2, and MnCl2 in NaOH-H2O solutions and study of lithium recovery from seawater via two-stage precipitation process, Hydrometallurgy 146 (2014) 142–148.
[42] R.R. H, A. A.-N, R. A.-Z, A. Alhozaimy, D.D.N. Singh, Effect of simulated concrete pore solution chemistry, chloride ions, and temperature on passive layer formed on steel reinforcement, ACI Mater. J. 111 (4) (2014).
[43] B. Ersoy, S. Dikmen, T. Uygunoğlu, M.G. İçduygu, T. Kavas, A.J.S. Olgun, E.o. C. Materials, Effect of mixing water types on the time-dependent zeta potential of Portland cement paste, Sci. Eng.Compos.Mater. 20 (3) (2013) 285–292.
[44] Y. Jin, D.J. Stephan, Hydration kinetics of Portland cement in the presence of vinyl acetate ethylene latex stabilized with polyvinyl alcohol, J. Mater.Sci. 53 (10) (2018) 7417–7430.
[45] K. Natkunarajah, K. Masilamani, S. Maheswaran, B. Lothenbach, D.A. S. Amarasinghe, D. Attygalle, Analysis of the trend of pH changes of concrete pore solution during the hydration by various analytical methods, Cement Concr. Res. 156 (2022), 106780.
[46] G. Plusquellec, M.R. Geiker, J. Lindgård, J. Duchesne, B. Fournier, K. De Weerdt, Determination of the pH and the free alkali metal content in the pore solution of concrete: Review and experimental comparison, Cement Concr. Res. 96 (2017) 13–26.
[47] B. Lothenbach, G. Le Saout, E. Gallucci, K. Scrivener, Influence of limestone on the hydration of Portland cements, Cement Concr. Res. 38 (6) (2008) 848–860.
[48] J. Williamson, O.B. Isgor, The effect of simulated concrete pore solution composition and chlorides on the electronic properties of passive films on carbon steel rebar, Corrosion Sci. 106 (2016) 82–95.
[49] M. Morcillo, B. Chico, J. Alcantara, I. Diaz, R. Wolthuis, D. de la Fuente, SEM/Micro-Raman characterization of the morphologies of marine atmospheric corrosion products formed on mild steel, J. Electrochem. Soc. 163 (8) (2016) C426–C439.
[50] P. Ghods, O.B. Isgor, G.J.C. Carpenter, J. Li, G.A. McRae, G.P. Gu, Nano-scale study of passive films and chloride-induced depassivation of carbon steel rebar in simulated concrete pore solutions using FIB/TEM, Cement Concr. Res. 47 (2013) 55–68.
[51] P. Ghods, O.B. Isgor, J.R. Brown, F. Bensebaa, D. Kingston, XPS depth profiling study on the passive oxide film of carbon steel in saturated calcium hydroxide solution and the effect of chloride on the film properties, Appl. Surf. Sci. 257 (10) (2011) 4669–4677.
[52] M. Hanesch, Raman spectroscopy of iron oxides and (oxy)hydroxides at low laser power and possible applications in environmental magnetic studies, Geophys. J. Int. 177 (3) (2009) 941–948.
[53] M. Bouchard, D. Smith, Catalogue of 45 reference Raman spectra of minerals concerning research in art history or archaeology, especially on corroded metals and coloured glass, Spectrochim. Acta A Mol. Biomol. 59 (10) (2003) 2247–2266.
[54] O.N. Shebanova, P. Lazor, Raman spectroscopic study of magnetite (FeFe2O4): a new assignment for the vibrational spectrum, J. Solid State Chem. 174 (2) (2003) 424–430.
[55] L.V. Gasparov, D.B. Tanner, D.B. Romero, H. Berger, G. Margaritondo, L. Forro, Infrared and Raman studies of the Verwey transition in magnetite, Phys. Rev. B 62 (12) (2000) 7939–7944.
[56] I. Chamritski, G. Burns, Infrared-and Raman-active phonons of magnetite, maghemite, and hematite: a computer simulation and spectroscopic study, J. Phys. Chem. B 109 (11) (2005) 4965–4968.
[57] M.A. Legodi, D. de Waal, The preparation of magnetite, goethite, hematite and maghemite of pigment quality from mill scale iron waste, Dyes Pigments 74 (1) (2007) 161–168.
[58] M.I. Dar, S. Shivashankar, Single crystalline magnetite, maghemite, and hematite nanoparticles with rich coercivity, RSC Adv. 4 (8) (2014) 4105–4113.
[59] S. Joiret, M. Keddam, X. Nóvoa, M. Pérez, C. Rangel, H. Takenouti, Use of EIS, ring-disk electrode, EQCM and Raman spectroscopy to study the film of oxides formed on iron in 1 M NaOH, Cem. Concr. Compos. 24 (1) (2002) 7–15.
[60] M. Ryan, R. Newman, G. Thompson, An STM study of the passive film formed on iron in borate buffer solution, J. Electrochem. Soc. 142 (10) (1995) L177–L179.
[61] P. Dawson, C.D. Hadfield, G.R. Wilkinson, The polarized infra-red and Raman spectra of Mg(OH)2 and Ca(OH)2, J. Phys. Chem. Solid. 34 (7) (1973) 1217–1225.
[62] P. Emayavaramban, S.G. Babu, R. Karvembu, K. Kadirvelu, N.J. Dharmaraj, nanotechnology, Gold nanoparticles supported on magnesium oxide nanorods for oxidation of alcohols, J. Nanosci. Nanotechnol. 16 (3) (2016) 2517–2526.
[63] A. Suslu, K. Wu, H. Sahin, B. Chen, S. Yang, H. Cai, T. Aoki, S. Horzum, J. Kang, F. M.J.S.r. Peeters, Unusual dimensionality effects and surface charge density in 2D Mg (OH) 2, Sci. Rep. 6 (1) (2016) 1–7.
[64] T.S. Duffy, C. Meade, Y. Fei, H.-K. Mao, R.J. Hemley, High-pressure phase transition in brucite, Mg(OH)2, J. Am. Mineralog. 80 (3–4) (1995) 222–230.
[65] A. Köliö, M. Honkanen, J. Lahdensivu, M. Vippola, M. Pentti, Corrosion products of carbonation induced corrosion in existing reinforced concrete facades, Cement Concr. Res. 78 (2015) 200–207. Part B.
[66] F. Ewing, The crystal structure of lepidocrocite, J. Chem. Phys. 3 (7) (1935) 420–424.
[67] J. Shi, J. Ming, Y. Zhang, J. Jiang, Corrosion products and corrosion-induced cracks of low-alloy steel and low-carbon steel in concrete, Cem. Concr. Compos. 88 (2018) 121–129.
[68] B.R. Barat, T. Palomar, B. Garcia, D. De la Fuente, E. Cano, Composition and Protective Properties of Weathering Steel Artificial Patinas for the Conservation of Contemporary Outdoor Sculpture, 9th interim meeting of the ICOM-CC metals working group. METAL2016, New Delhi, India, 2016.
[69] Z. Ai, W. Sun, J. Jiang, D. Song, H. Ma, J. Zhang, D. Wang, Passivation characteristics of alloy corrosion-resistant steel Cr10Mo1 in simulating concrete pore solutions: combination effects of pH and chloride, Materials 9 (9) (2016) 749.
[70] J. Gui, T.M. Devine, Insitu vibrational-spectra of the passive film on iron in buffered borate solution, Corrosion Sci. 32 (10) (1991) 1105–1124.
[71] J.C. Rubim, J. Dünnwald, Enhanced Raman scattering from passive films on silver-coated iron electrodes, J. Electroanal. Chem. Interfacial Electrochem. 258 (2) (1989) 327–344.
[72] C.N. Lininger, C.A. Cama, K.J. Takeuchi, A.C. Marschilok, E.S. Takeuchi, A.C. West, M.S. Hybertsen, Energetics of lithium insertion into magnetite, Defect. Magnet. Maghem. 30 (21) (2018) 7922–7937.
[73] J. Chen, K. Huang, S. Liu, Hydrothermal preparation of a protective Fe3O4 film on Fe foil, Corrosion Sci. 50 (7) (2008) 1982–1986.
[74] M. Brady, G. Rother, L. Anovitz, K. Littrell, K. Unocic, H. Elsentriecy, G.-L. Song, J. Thomson, N. Gallego, B.J. Davis, Film breakdown and nano-porous Mg (OH) 2 formation from corrosion of magnesium alloys in salt solutions, J.Electrochem.Soc. 162 (4) (2015) C140.
[75] M.E. Kirby, J.C. Bullen, M. Hanif, H.F. Heiba, F. Liu, G.H. Northover, E. Resongles, D.J.J. Weiss, Determining the Effect of pH on Iron Oxidation Kinetics in Aquatic Environments: Exploring a Fundamental Chemical Reaction To Grasp the Significant Ecosystem Implications of Iron Bioavailability, J. Chem. Educ. 97 (1) (2019) 215–220.
[76] Y.-J. Du, Y.-L. Bo, F. Jin, C.-Y.J. Liu, C. Engineering, Durability of reactive magnesia-activated slag-stabilized low plasticity clay subjected to drying–wetting cycle, Eur. J.Environ. Civ.Eng. 20 (2) (2016) 215–230.
[77] N.T. Dung, C. Unluer, Improving the carbonation of reactive MgO cement concrete via the use of NaHCO 3 and NaCl, J. Mater. Civ. Eng. 30 (12) (2018), 04018320.
[78] N.T. Dung, T.J.N. Hooper, C. Unluer, Improving the carbonation resistance of Na2CO3-activated slag mixes via the use of reactive MgO and nucleation seeding, Cem. Concr. Compos. 115 (2021), 103832.